International Academic Institute for Science and Technology

International Academic Journal of Science and Engineering
Vol. 9, No. 2, 2022, pp. 37-45.

ISSN 2454-3896

International Academic Journal of Science and Engineering

www.iaiest.com

Synthesize and Characterization of Cerium Oxide Nanostructure for Oxidizing Gas Sensor Application

Mais Talib Kareem [a], Suhad A. Hamdan [b]

[a] *Department of Physics, College of Science, University of Baghdad, Baghdad, Iraq.*
E-mail: Mais.taleb1204a@sc.uobaghdad.edu.iq
[b] *Department of Physics, College of Science, University of Baghdad, Baghdad, Iraq.*
E-mail: Suhad.a@sc.uobaghdad.edu.iq

Abstract

The films were synthesized made on a seeded layer using the hydrothermal technique. The impact of pH on ceria's characterization was explored, two samples synthesis ceria acidic (pH = 4) and ceria basic (pH = 10).

The XRD, AFM, FE-SEM, UV-visible, The DC conductivity and gas sensing properties of the thin films prepared were explored. The films were polycrystalline, with crystallite sizes of (10.4-43) nm for ceria basic and (20.90-44.263) nm for ceria acidic, and an FCC structure, that according XRD analysis. Ceria (CeO_2) nanostructures were evaluated as their gas sensing characteristics, around (123.1563%) at T=473°K when exposed to the oxidizing gas NO_2 with (3.291) sec and (34.019) sec for both rise and fall times respectively.

Keywords: Ceria, Hydrothermal, Gas Sensor, CeO_2.

DOI: 10.9756/IAJSE/V9I2/IAJSE0912
Received: 16 March 2022/Revised: 22 April 2022/Accepted: 23 May 2022/Published: 30 June 2022

Introduction

Cerium has the atomic number 58 and the symbol Ce in the periodic table's lanthanide series. It is classified as a rare earth element. It is the rarest earth element, with the highest concentration [1, 2]. Cerium must be stored in a controlled atmosphere since it oxidizes easily in the air at ambient temperature to ceria (cerium dioxide). Cerium is a semiconductor with a broadband gap. It forms oxides (Ce_2O_3, CeO_2) in two oxidation states (Ce +three, cerous) and (Ce +four, ceric) [3,4]. Cerium oxide is insoluble in water, melts at (2500-2600)ºC, has a molecular weight of 172.12g/mole, and is available as a pale-yellow or brownish powder [5]. It features a fluorite-like cubic structure in which each cerium site is surrounded by eight oxygen sites in a face-centered cubic (FCC) arrangement, with a tetrahedron cerium site on each oxygen site [6]. Nano ceria is currently extensively applied in sensing applications, particularly in gas and electrochemical sensors. Several methods are used to produce cerium oxide nanoparticles, including hydrothermal, sol-gel, flame spray, pyrolysis, and solvothermal techniques [7]. In this work Hydrothermal synthesis is used for synthesis the films. The process of creating complex nanostructures by depending on mineral solubility in hot environments under high stress, with crystal development taking place in a device consisting of a metal strain vessel known as a crystal boom and an autoclave. [8].

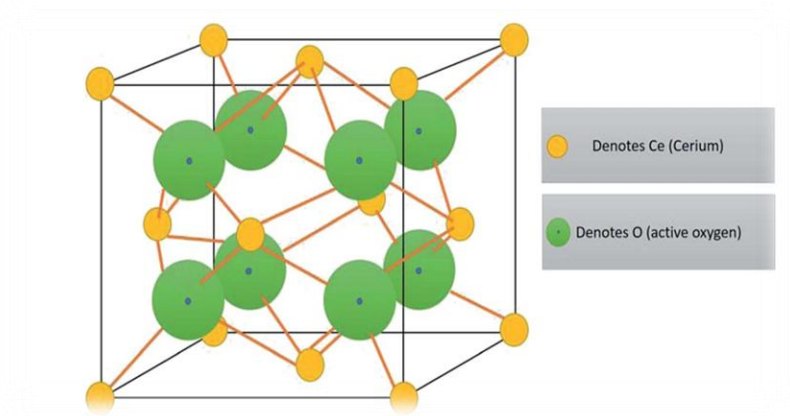


Figure 1: Cerium Oxide (CeO_2) Nanoparticles have a Face-centered Cubic Structure in General

Experimental

Hydrothermal technique was used to make cerium oxide thin films on a seeded layer. To begin, $CeC_{l3.6}H_2O$ at (0.2M) will be dissolved in 40 mL methanol and 5 mL citric acid will be dissolved in 40 mL distilled water to make the seeded layer. The aqueous solutions of cerium chloride and citric acid are stirred separately for 10 minutes on a magnetic stirrer. To synthesize the precursors, which are cerium oxide ion sources, the citric acid was added carefully to the aqueous solution of cerium chloride with stirrer and PH is measured (PH= 4.3). The resultant solution was spin coated for 20 seconds at 2000 rpm onto silicon and glass substrates, and the process was repeated numerous times to get the necessary seed layer thickness. These seeded layers are then heat annealed for 2 hours at 300°C to increase crystallinity and remove impurities, and the sample is now ready for the next stage, which is the growth process. To make the growth solution, combine 0.2 M cerium chloride (as a source of cerium ions) and 0.175gm Hexamine $C_6H_{12}N_4$ (as an oxidizing agent) in distilled water and stir for 10 minutes. After that, the two solutions are then combined and stirred for 10 minutes. Inside the Teflon container, the seeded layers were vertically aligned, and the mixture was placed in a stainless-steel autoclave lined with Teflon. The autoclave was used for an electronic temperature-controlled oven was closed and kept at 120°C for three hours. The autoclave was then allowed to spontaneously cool to ambient temperature. After washing the substrates with distilled water to remove any remaining solid particles or unreacted atoms, the sample is dried in an oven at 100ºC for 30 minutes. The annealing technique will be carried out in a furnace at 500ºC for one hour .

The above steps have been done but ammonia is added to the solution, and the pH is measured and controlled to a value of 10 or until the color of solution changes from purple to convert milky, we get CeO_2 from basic solution.

The films are now available for characterization. X-ray diffraction (XRD) is used to determine structural characteristics using (XRD- 6000 Labx, supplied by Shimadzu, X-ray source is Cu) within the wavelength range of (190-1100) nm, optical absorption spectra were acquired using the UV–VIS spectrophotometer "OPTIMA SP-3000". The morphology was characterized by field emission scanning electron microscopy (FESEM) with type by Inspect

F50 FESEM, FEI company, made in Holland. AFM atomic force macroscopy is used to determine the topography surface and thickness of cerium oxide CeO_2 (model TT-2 AFM workshop). D.C. Conductivity was done by the temperature recorded by (MANFREDI L7), the bias voltage was supplied by (FARNELL E350) power supply, the current read out by ("USA origin, Kithley-616 Digital Electrometer") multimeter. Electrical resistance can be measured directly for all steps with digital electrometer.

Results and Discussion

1. XRD Study

The XRD patterns confirm the polycrystalline nature of the cerium oxide nanoparticles, were show in figure (2) which had a face-centered cubic structure. XRD testing of synthetic cerium oxide grown on silicon substrates.

The obtained 2θ for CeO_2 basic (28.63º, 33.09º, 47.56º, 56.27º, 59.27º, 76.700°, and 79.070º) referred to (111, 200, 220, 311, 222, 331 and 420) planes respectively, which match well with standard values of CeO_2 (ASTM) card number 00-034-0394 and it is same as the previous researches [9,10], and for CeO_2 acidic 2θ~(28.63º,33.082º, and 47.479°) referred to (111), (200), and (220) planes respectively, which agreement with standard values of CeO_2 (ASTM)card number 00-043-1002. Exhibit preferred orientation along the (111) for CeO_2 basic and CeO_2 acidic, the (111) peak that is enhanced as the extent of alignment increases for CeO_2 basic. Estimates the average Crystallite size (D) using Scherer's formula equation [11]:

$$D = k\,\lambda / \beta \cos\theta \qquad (1)$$

Where K is the shape factor (0.94), λ is the x-ray source's wavelength (0.15405 nm), β is the diffraction peak's full width at half-maximum (FWHM) and (θ)is the diffraction peak's angle. The average crystallite size value was found in the range (10-43) nm for CeO_2 basic sample and (20.90-44.263) nm for CeO_2 basic sample. In general D for CeO_2 basic sample shorter than CeO_2 acidic. The shortest D for CeO_2 basic sample at 200 plane is equal to 10. 4166nm.we have also observed the improvement in crystallinity of CeO_2.

From the following equation is used to derive the lattice constant (a) [12]:

$$d_{hkl} = \frac{a}{\sqrt{h^2+k^2+l^2}} \qquad (2)$$

Where (h, k, l) is the plane index of the crystal and d_{hkl} is the interplanar spacing, which is determined by the Bragg's law [13]:

$$n\lambda = 2d_{hkl} \sin\theta \qquad (3)$$

The results of D and d_{hkl} are tabled in table (1). The crystallite size increased from 10 to 45 nm with increase the PH. It must be noted that the crystallite size increases gradually with increasing Ph and crystal growth becomes sharp at PH=10, it may be assumed that the particles grow mainly because of an interfacial reaction. The lattice constant of the samples is slightly higher compared to the bulk counter parts due to its increased oxygen vacancies Table (1)**:** The structural parameters for cerium oxide.

Table 1: Structure Parameters for Cerium Oxide Thin Films Deposited on p-Si

CeO_2 Basic	**2θ(deg.)**	**FWHM (deg.)**	**d_{hkl} Exp.(A°)**	**D_{ave}(nm)**	**hkl**	**d_{hkl} Std.(A°)**	**Card No**
0.2 M	28.63	0.3936	3.11672	20.9088	111	3.1234	00-034-0394
	33.09	0.7986	2.7061	10.4166	200	2.706	00-034-0394
	47.56	0.7986	1.9111	10.9111	220	1.9132	00-034-0394
	56.27	0.2952	1.6342	30.63	311	1.6316	00-034-0394
	59.27	0.2952	1.5584	31.0751	222	1.5621	00-034-0394
	76.7	0.3993	1.2419	25.4594	331	1.2414	00-034-0394
	79.07	0.2400	1.2105	43.0711	420	1.2101	00-034-0394
CeO_2 Acidic	**2θ(deg.)**	**FWHM (deg.)**	**d_{hkl} Exp.(A°)**	**D_{ave}(nm)**	**hkl**	**d_{hkl} Std.(A°)**	**Card No**
0.2M	28.63	0.3936	3.11672	20.9088	111	3.1234	00-034-0394
	33.082	0.1968	2.7069	42.2689	200	2.7056	00-043-1002
	47.479	0.1968	1.9191	44.2630	220	1.9134	00-043-1002

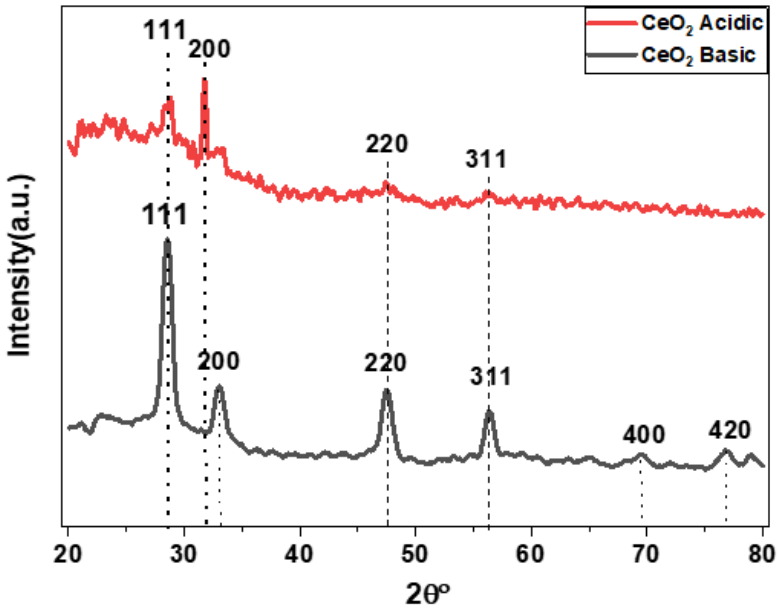
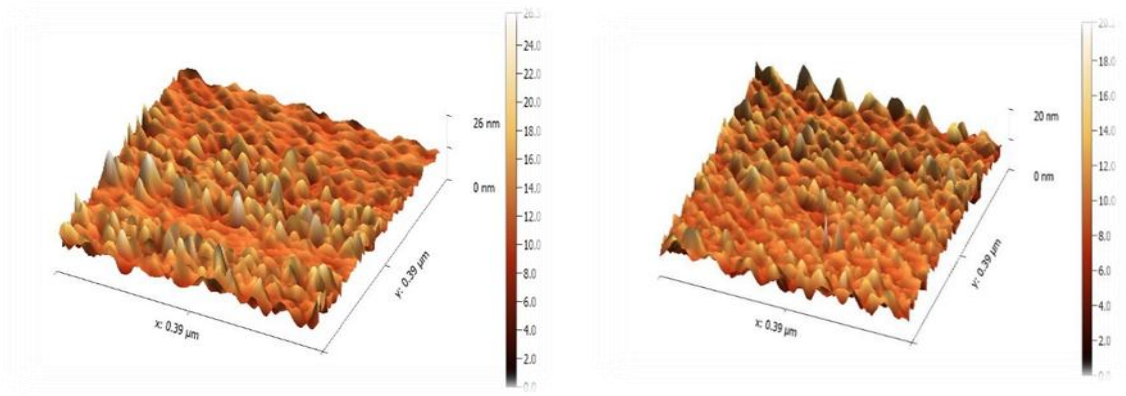


Figure 2: The XRD Patterns of Basic and Acidic CeO_2

2. AFM Analysis

The topography surface of cerium oxide CeO_2 phases were tested by AFM analysis to offer a large surface inspection of microstructural arrays. Figure (3) show the images with (3D) for samples.



(a) **(b)**

Figure 3: (A) and (B) 3-D Images of CeO_2 Basic and Acidic Respectively

Topography parameters contain surface area, average dimeter, root mean square (RMS), thickness, and roughness for samples are tabulated as can be seen in Table 2. From the results notice cerium Oxide basic has high thickness, high average dimeter, and high roughness. Roughness can be generally observed as one of the significant parameters. The surface roughness not merely describes the scattering of the light, but also provides information on quality of the studied surface.

Table 2: Surface Area, Average Dimeter, Thickness, (RMS) and Roughness (nm) of Cerium Oxide for Two Samples

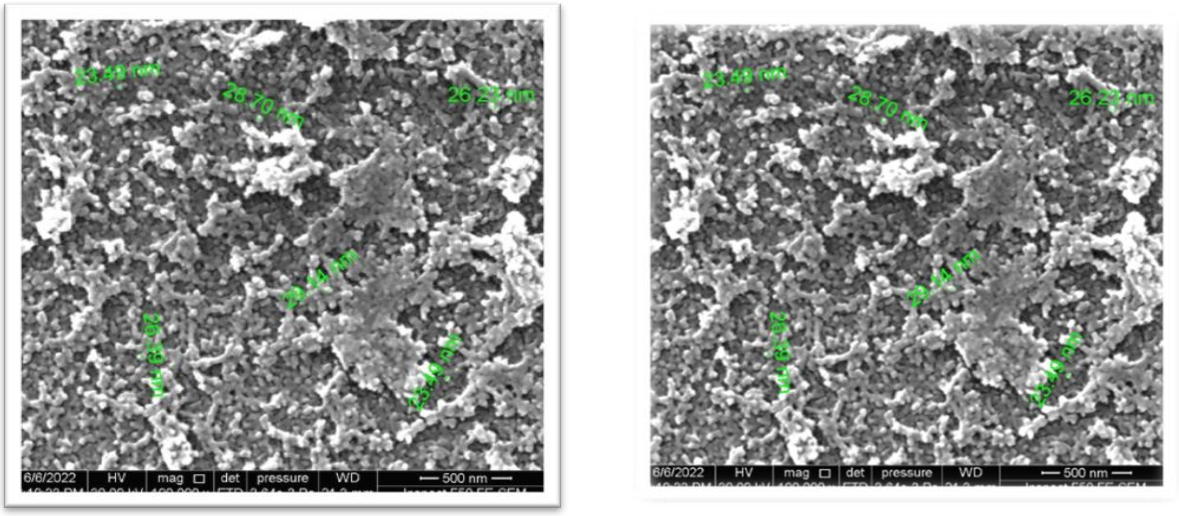
sample	RMS (nm)	Average dimeter (nm)	surface area(μm^2)	Thickness (nm)	Roughness (nm)
CeO_2 Basic	2.86	25.02	1.30527	228.6	24.75
CeO_2 Acidic	2.74	17.67	1.29953	118.5	13.31

3. Field Emission Scanning Electron Microscope (FE-SEM)

FE-SEM can be used for various purposes, such as: studying the growth mechanisms of the deposit, morphological changes in the morphology as a function of deposition parameters, presence, and properties of particulates.

Figure (4a) (0.2A) show nanoparticles having uniform size are observed with aggregate of nanoparticles without crack (23.49-29.14nm). Figure (4b) (0.2 B) shows that the image of samples higher precursor concentration gives much smaller, uniform nanoparticles with agglomeration (13.13-14.03nm). Precursor concentration has a prominent role in the formation of uniform and small size cerium oxide nanoparticles. These analyses show that high homogeneity emerged in the samples surface by pH. Perhaps this is related to the roughness of the surface, as we noticed from the examination AFM. The results show that the morphology of the particles changes to the spherical shape with less agglomeration by increasing PH. FE-SEM images of as prepared at pH=10 show the agglomeration of small crystallites and are attributed to uncontrolled coagulation during precipitation, at higher pH, small crystallites are clinging together to form a large agglomerated spheroidal structure.

Figure (4b): Show The grains distribution of nanoparticles ranged between (10-30) nanometers and was more distributed at 19 nanometers for (0.2 basic CeO_2), and for (0.2 acidic CeO_2) the grains distribution range between (20-60) nanometers and was more distribution at (27) nm.



(a) **(b)**

Figure 4a: FE-SEM Images at (500 nm Scale) of Cerium Oxide Thin Film for (0.2 Basic) and (0.2 Acidic)

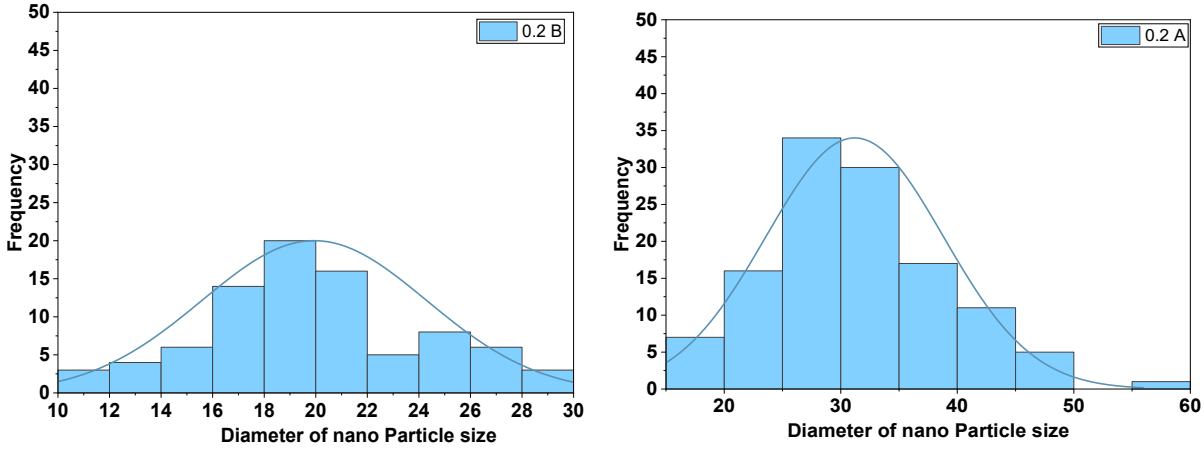


Figure 4b: The Grains Distribution of Nanoparticles CeO_2

4. Optical Properties

UV-vis absorption spectroscopy was used to evaluate the optical properties of the CeO_2 basic and CeO_2 acidic nanostructures. (Fig. 5a) shows the absorption spectra of samples, the absorption spectra reveal Samples of CeO_2 nanostructure have significantly higher absorption in the ultraviolet light region and blue shifted. Absorbance peak was observed around 310 nm for CeO_2 basic and 315 for CeO_2 acidic agreement with [14].

The charge-transfer between the O 2p and Ce 4f states in O^{2-} and Ce^{4+}, which is much greater than the $4f^1$-$5d^1$ transition from the Ce^{3+} species in the mixed valence ceria system, causes CeO_2 absorption in the UV region. The spectra show that the CeO_2 acidic nanostructure possesses higher light absorption intensity.

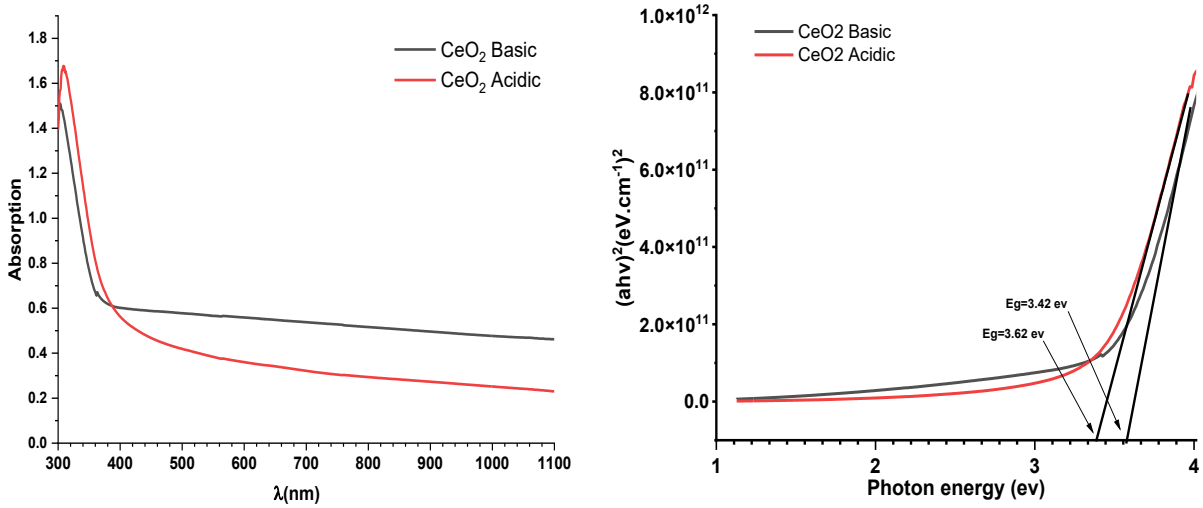
Fig. 5b shows the band gap was estimated from Tauc relation can be used to obtain the direct band gap value [13].

$$(\alpha h\upsilon)\mathrm{r} = \mathrm{B}(\mathrm{h}\upsilon - \mathrm{Eg}) \qquad (4)$$

Where $h\upsilon$ is the photon energy in eV, α is the absorption coefficient in cm^{-1}, B is a material-related constant, while the value of r is 1/2 for a direct transition, a plot of $(ah\upsilon)^r$ versus $h\upsilon$ reveals the energy intercept Eg.

Ceria is a semiconductor with a direct band gap as usually done by other researchers [9,15,16]. We notice the optical energy gap are 3.62eV agreement with [17] and 3.42 eV for CeO_2 basic and acidic samples respectively.

These values are higher than those obtained in bulk CeO_2 nanoparticles. CeO_2 has a bulk band gap of (3.19 eV) [18]. It means that as compared to bulk CeO_2, the band gap energy of nanocrystalline CeO_2 increases, and that this increase is attributable to charge carrier quantum confinement in the CeO_2 nano system. As a result, the absorption band shifts to a higher energy range, resulting in a blue shift.



(a) **(b)**

Figure 5: UV-vis Absorption Spectra of Cerium Oxide Nanostructure (a) Absorption (b) Optical Band Gap

5. DC Conductivity

The DC electrical conductivity of the cerium oxide thin films with concentration (0.2M) and different pH (pH=4.3 for CeO_2 acidic, pH=10 for CeO_2 basic) was measured as a function of temperature in the range temperature (293-393) K. It is very useful to determine the activation energy.

The activation energy and conductivity at room temperature of the cerium oxide films is determined using eq. (5) and from slope of the linear plots of the Ln σ versus 1000/T, as shown in fig (6).

$$\sigma(T) = \sigma_o \exp\left(-\frac{E_a}{K_B T}\right) \quad (5)$$

Where σ is conductivity at temperature T, σ_o is a constant, K_B is the Boltzmann constant, T is the absolute temperature and E_a is the activation energy. Figure (5) shows that films have two activation energies one in low temperature region and the other in high temperature region this confirm polycrystalline structure nature this agreement with XRD examination.

As the temperature increases, the conductivity increases as well. Table 3 shows that at the same temperature, the electrical conductivity values of basic ceria are higher than those of acidic ceria.

Ceria is a mixed ionic–electronic conductor that transports electrons through n-type tiny polaron hopping and oxygen ions through oxygen vacancies, as is well known. These are influenced by the surrounding gas phase's doping level, temperature, and oxygen partial pressure. Ceria is largely reduced ($Ce^{4+} \rightarrow Ce^{3+}$) and has a predominantly electronic conduction at low oxygen partial pressure and raised temperature (approximately 900°K), but it is predominantly ionic at high oxygen partial pressure and intermediate temperature [19,20].

The linear dependence indicates thermally activated mechanisms of electrical conductivity with two activation energies (Ea_1=0.0447-0.2462) eV and (Ea_2=0.1718-0.1381) eV for basic and acidic ceria, respectively. This could be conduction mechanisms such as ionic and small polaron hopping, which both require an activation energy.

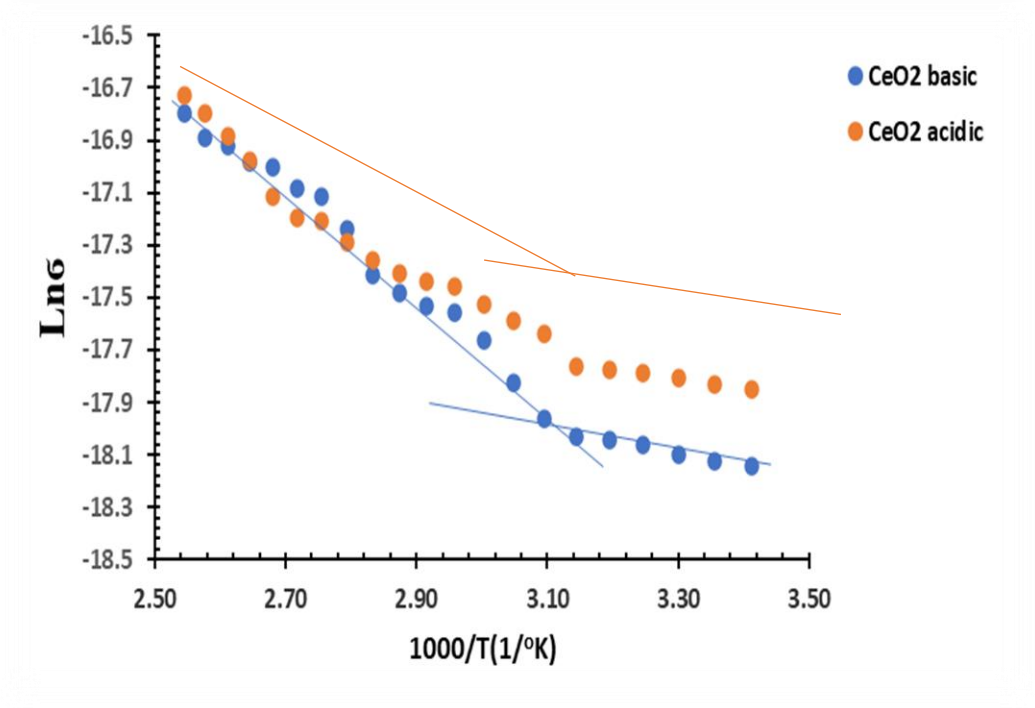


Figure 6: Changes in Ln (σ) as a Function of Reciprocal Temperature for Basic and Acidic CeO_2

Table 3: Electrical Characteristics of Ceria Basic and Acidic

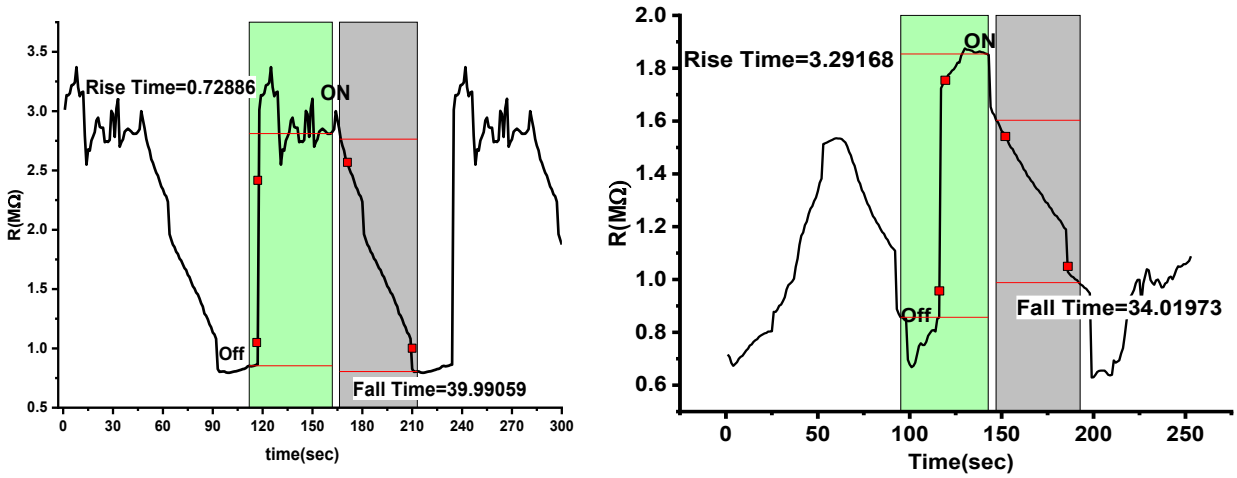
sample	E_{a1} (eV)	Range (K)	E_{a2} (eV)	Range (K)	σ_{RT} ($\Omega^{-1}.cm^{-1}$)
CeO_2 basic	0.045	293-323	0.172	323-393	1.32E-08
CeO_2 acidic	0.246	293-318	0.138	318-393	1.77E-08

Gas Sensor

The sensing properties of CeO_2 nanoparticles and the temperature dependency of the sensitivity against oxidizing gas (NO_2) deposited on p-Si substrates is evaluated as a function of time and operating temperature.

1. NO_2 Sensing Mechanism for Prepared Sensors

The gas used here can be classified as an oxidizer, NO_2 because it accepts electrons from the metal oxide surface. Figures (7) exhibit the variation of resistance as a function of time for CeO_2 basic and acidic sensors with an ON/OFF gas valve, after exposure to NO_2 at various operating temperatures ranging from room temperature to 473°K gradually, with the best sensitivity at 473°K.



(a) **(b)**

Figure 7: Resistance Changes with Time for CeO_2 Sensors Against NO_2 Gas at Different Operating Temperature. (A) CeO_2 Acidic Deposited on P-Si at T=473°K Against NO_2. (B) CeO_2 Basic Deposited on P-Si at T=473°K Against NO_2

Previous figure shows the resistance values increased when the films were exposed to NO_2 gas (Gas ON), then decreased when the gas was turned off (Gas OFF). Results shows a decreasing resistance with increasing temperature which.

The reason for such behavior may be attributed to the fact that the molecules of the oxygen on the metal oxide surface gains the electrons from metal oxides and form the ions of the oxygen. The surfaces of the metal oxide have a hole layer of accumulation for P-type and layer of the electron depletion for n-type. In the case where the oxidizing gases are generated, the resistance of n-type metal oxide gas sensor increasing because of increasing the thickness of the electron depletion layer**.** When oxidizing gases are introduced, the thickness of the electron depletion layer increases. Thus, the resistance of the n-type metal oxide gas sensor has increased. Relatively speaking, the resistance of the P-type metal oxide gas sensor decreased due to the increase in the hole accumulating layer. When reducing gases are introduced, the resistance of the p-type metal oxide gas sensor increases due to the decrease of the hole accumulating layer the sensitivity can be calculated as given as [21]:

$$S= | (R_g- R_a) /R_a| * 100\% \quad (6)$$

S: represents sensitivity, R_a and R_g: represent the film's electrical resistance in air and the existence of the gas, respectively. The sensitivity of ceria basic is higher than acidic may be ceria basic more roughness surface than ceria acidic this confirms the AFM analysis.

Results of rise time, fall time, and sensitivity results show in table 4.

Table 4: Results of Rise Time, Fall Time, and Sensitivity for Gas Sensor

Sample	Rise time(sec)	Fall time(sec)	Sensitivity %
CeO_2 basic	3.29168	34.01973	123.1563%
CeO_2 acidic	0.72886	39.99059	74.30578%

Conclusion

Hydrothermal method has been successfully established for the preparation of nanostructure ceria basic and acidic. The XRD measurements shows that the films are polycrystalline in face center cubic structure. The Crystallite size of basic ceria film less than acidic ceria. The AFM measurements from the results notice cerium Oxide basic has high thickness, high average dimeter, and high roughness. The FE-SEM show (CeO_2 Acidic) nanoparticles having uniform size are observed with aggregate of nanoparticles without crack (23.49-29.14nm), (CeO_2 Basic) shows that the image of samples higher precursor concentration gives much smaller, uniform nanoparticles with agglomeration (13.13-14.03nm). The Ceria films showed a strong UV–vis absorption below 400 nm, the direct band gap was found 3.62 eV and 3.42 eV for basic and acidic ceria respectively. Optical energy gap of prepared films has blue shift with

respect to bulk ceria, this an indication that a quantum confinement happened, and the particle size decreased. DC electrical conductivity measurement for ceria nanostructure proves the semiconducting nature of synthesized thin films and follows small polaron hopping and oxygen ions. The sensor based on a nanostructure of basic and acidic ceria exhibited the best performance for NO_2 detection. But the sensitivity of ceria basic is higher than acidic a nanostructured sensor It was found that PH of the sensors affect the material sensitivity.

References

Yang, C. (2016). Spectroscopic Studies of Surface Chemistry on Cerium Oxide.

Rajeshkumar, S., & Naik, P. (2018). Synthesis and biomedical applications of cerium oxide nanoparticles–a review. *Biotechnology Reports, 17*, 1-5.

Tang, C.C., Bando, Y., Liu, B.D., & Golberg, D. (2005). Cerium oxide nanotubes prepared from cerium hydroxide nanotubes. *Advanced Materials, 17*(24), 3005-3009.

Dahle, J.T., & Arai, Y. (2015). Environmental geochemistry of cerium: applications and toxicology of cerium oxide nanoparticles. *International journal of environmental research and public health, 12*(2), 1253-1278.

Schwarz, K. (2006). Materials design of solid electrolytes. *Proceedings of the National Academy of Sciences, 103*(10), 3497-3497.

Kumar, E., Selvarajan, P., & Muthuraj, D. (2013). Synthesis and characterization of CeO_2 nanocrystals by solvothermal route. *Materials Research, 16*, 269-276.

Chopra, K. (2012). *Thin film device applications.* Springer Science & Business Media.

Zhu, X., Hou, K., Chen, C., Zhang, W., Sun, H., Zhang, G., & Gao, Z. (2015). Structural-controlled synthesis of polyaniline nanoarchitectures using hydrothermal method. *High Performance Polymers, 27*(2), 207-216.

Khadar, Y.S., Balamurugan, A., Devarajan, V.P., Subramanian, R., & Kumar, S.D. (2019). Synthesis, characterization and antibacterial activity of cobalt doped cerium oxide (CeO_2: Co) nanoparticles by using hydrothermal method. *Journal of Materials Research and Technology, 8*(1), 267-274.

Farahmandjou, M., Zarinkamar, M., & Firoozabadi, T.P. (2016). Synthesis of Cerium Oxide (CeO2) nanoparticles using simple CO-precipitation method. *Revista mexicana de fisica, 62*(5), 496-499.

Ali, I.M., & Ibrahim, I.M. (2021). Toxic Gas Response for Nanostructured Cobalt Oxide Thin Films. *Iraqi Journal of Physics (IJP), 19*(50), 20-30.

Hamdan, S.A., & Ali, I.M. (2019). Enhancement of Hydrothermally Co_3O_4 Thin Films as H2S Gas Sensor by Loading Yttrium Element. *Baghdad Science Journal*, *16*(1 Supplement).

Hamdan, S.A. (2019). Synthesized pure cobalt oxide nanostructure and doped with yttrium by hydrothermal method for photodetector applications. *Iraqi Journal of Physics, 17*(40), 77-87.

Prabaharan, D.M.D.M., Sadaiyandi, K., Mahendran, M., & Sagadevan, S. (2016). Structural, optical, morphological and dielectric properties of cerium oxide nanoparticles. *Materials Research, 19*, 478-482.

Ni, X., Zhao, Q., Zhou, F., Zheng, H., Cheng, J., & Li, B. (2006). Synthesis and characterization of NiO strips from a single source. *Journal of Crystal Growth, 289*(1), 299-302.

Hogarth, C.A., & Al-Dhhan, Z.T. (1986). Optical absorption in thin films of cerium dioxide and cerium dioxide containing silicon monoxide. *Physica Status Solidi. B, Basic Research, 137*(2), K157-K160.

Khadar, Y.S., Balamurugan, A., Devarajan, V.P., Subramanian, R., & Kumar, S.D. (2019). Synthesis, characterization and antibacterial activity of cobalt doped cerium oxide (CeO_2: Co) nanoparticles by using hydrothermal method. *Journal of Materials Research and Technology, 8*(1), 267-274.

Liao, X.H., Zhu, J.M., Zhu, J.J., Xu, J.Z., & Chen, H.Y. (2001). Preparation of monodispersed nanocrystalline CeO_2 powders by microwave irradiation. *Chemical Communications,* (10), 937-938.

Lavik, E.B., Kosacki, I., Tuller, H.L., Chiang, Y.M., & Ying, J.Y. (1997). Nonstoichiometry and Electrical Conductivity of Nanocrystalline CeO $${2-x} $$. *Journal of Electroceramics, 1*(1), 7-14.

Konysheva, E., & Irvine, J.T. (2011). Transport properties of multi-cations doped cerium oxide. *Solid State Ionics, 184*(1), 27-30.

Hamdan, S.A., IbrahiM, I.M., & Ali, I.M. (2020). Comparison of anatase and rutile TiO2 nanostructure for gas sensing application. *Digest Journal of Nanomaterials & Biostructures (DJNB),* 15(4).